# Supporting Information

# Activating Hematite Nanorod Photoanode via Fluorine-Doping and Further Surface Fluorination for Enhanced Oxygen Evolution Reaction

*Chenglong Wang,[a] Shenqi Wei,[a] Feng Li,[b] Xuefeng Long,[a] Tong Wang,[a] Peng Wang,[a] Shuwen Li,[a] Jiantai Ma[a] and Jun Jin*[a]*

[a]State Key Laboratory of Applied Organic Chemistry (SKLAOC), College of Chemistry and Chemical Engineering, Lanzhou University, Lanzhou 730000, (P. R. China). The Key Laboratory of Catalytic Engineering of Gansu Province and Chemical Engineering, College of Chemistry and Chemical Engineering, Lanzhou University, Lanzhou 730000, (P. R. China). [b]State Key Laboratory of High-efficiency Coal Utilization and Green Chemical Engineering, School of Chemistry and Chemical Engineering, Ningxia University, Yinchuan, Ningxia, 750021, P. R. China

**AUTHOR INFORMATION**

**Corresponding Author** * E-mail: jinjun@lzu.edu.cn.

## Equations related in this work

1. At room temperature, the applied bias was converted to the reversible hydrogen electrode (RHE) according to the equation below:

$$E_{\mathrm{RHE}} = E_{\mathrm{Ag/AgCl}} + E_{\mathrm{Ag/AgCl}}^{0} + 0.0591\ V \times \mathrm{pH} \qquad \text{equation 1}$$

$$(E_{\mathrm{Ag/AgCl}}^{0} = 0.1976\ \mathrm{V\ vs.\ RHE\ at\ 25\ ℃})$$

where $E_{\mathrm{RHE}}$ is the potential versus (vs.) RHE, $E_{\mathrm{Ag/AgCl}}$ is the experimental potential measured vs. the Ag/AgCl electrode[1].

2. Mott-Schottky (M-S) plots were generated under dark with a voltage of 20 mV at a frequency of 1 kHz. In the M-S plot, the flat band potential and the carrier densities of the photoelectrode are measured according to following equations[2]:

$$N_D = \frac{2}{e\varepsilon\varepsilon_0}\left[\frac{d(\frac{1}{C^2})}{dV}\right]^{-1} \qquad \text{equation 2}$$

Where, C is the space charge capacitance in the semiconductor (obtained from M-S curves), e is the electron charge, ε is the vacuum permittivity ($8.85\times10^{-12}$ F $m^{-1}$), $\varepsilon_0$ is the relative dielectric constant of hematite ($\varepsilon_0 = 80$), $N_D$ is the charge donor density ($cm^{-3}$), V is the electrode applied potential, $V_{fb}$ is the flat band potential, κ is the Boltzmann's constant ($1.38\times10^{-23}$ J $K^{-1}$) and T is the absolute temperature (K).

It is worth noting that the capacitance (C) is based on a flat structure, and therefore it is not suitable for our non-flat structure of the one-dimensional geometry nanorod arrays. In general, the comparison results of the flat structure and non-flat structure show that an underestimate of the donor density by 20% is achieved for the latter mode when it is considered as the former one. In this work, all the $Fe_2O_3$-based nanoarrays photoanodes are non-flat structure, thus the $N_D$ values for them are 20% larger than the experimental results calculated by equation[3].

3. Bulk charge separation and surface charge separation efficiency of the as-obtained photoanodes can be calculated using the following equations.

$$\eta_{\mathrm{bulk}} = J_{Na2SO3}/J_{abs} \qquad \text{equation 3}$$

$\eta_{surface} = J_{H2O}/J_{Na2SO3}$ equation 4

in which Jabs is the theoretical photocurrent density assuming that all absorbed photons can be converted into current (APCE = 100%), and $J_{H2O}$ and $J_{Na2SO3}$ are the photocurrent densities obtained in 1 M KOH aqueous solution without and with 1 M $Na_2SO_3$, respectively.

By integrating the overlapped areas between the UV-vis absorption spectrum and the AM 1.5G solar spectrum, assuming APCE=100%, the $J_{abs}$ of α-$Fe_2O_3$ was calculated to be 9.98 mA $cm^{-2}$.[4, 5] This value is suitable for α-$Fe_2O_3$, F-$Fe_2O_3$ and $FeF_x$/F-$Fe_2O_3$ due to the fact that the ability of light absorption was approximately the same for all the samples.

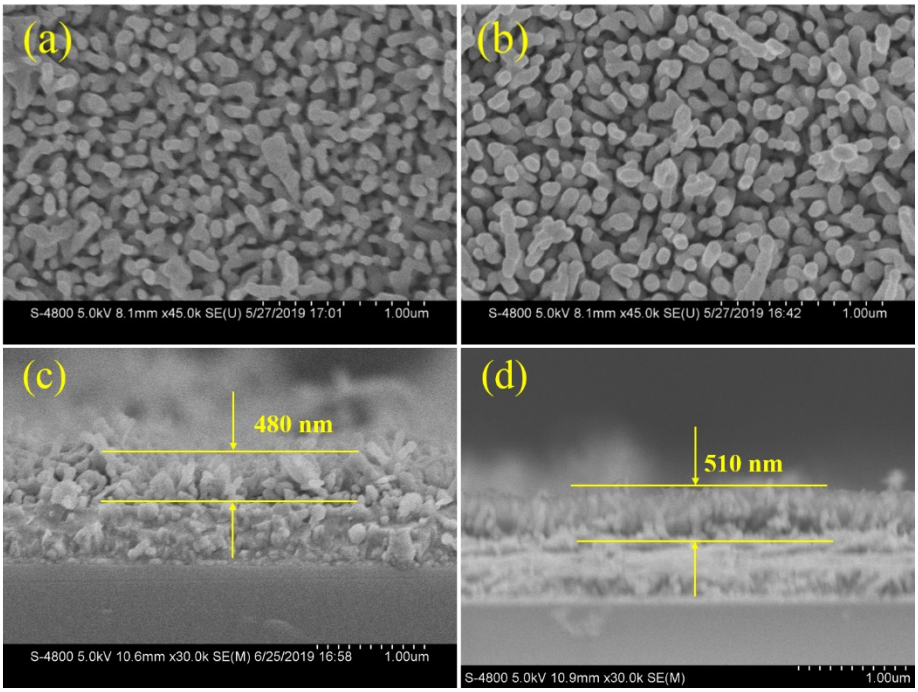


**Fig. S1** The top-view and Cross-section SEM images of α-$Fe_2O_3$ (a, c) and F-$Fe_2O_3$ (b, d) photoanodes.

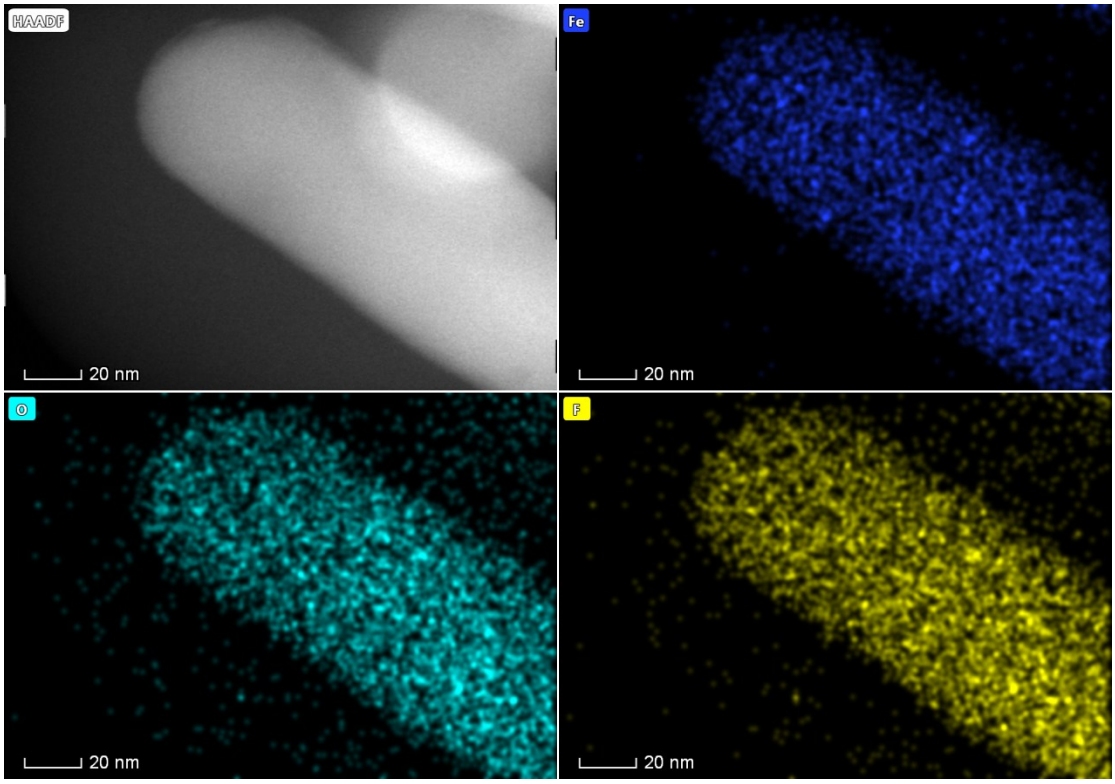


**Fig. S2** TEM-EDX element mapping for the F-$Fe_2O_3$ nanorod.

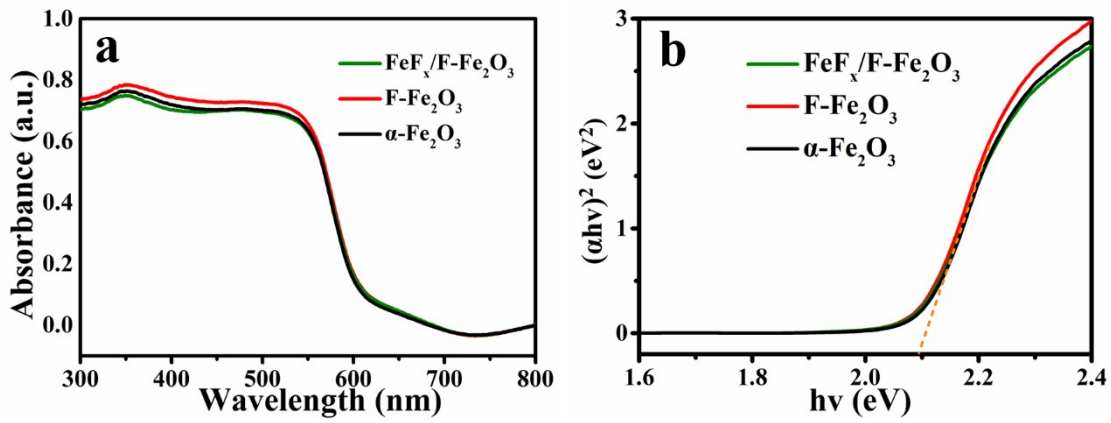


**Fig. S3** UV−visible diffuse reflection spectra (a) and the calculated band gaps (b) of each electrode.

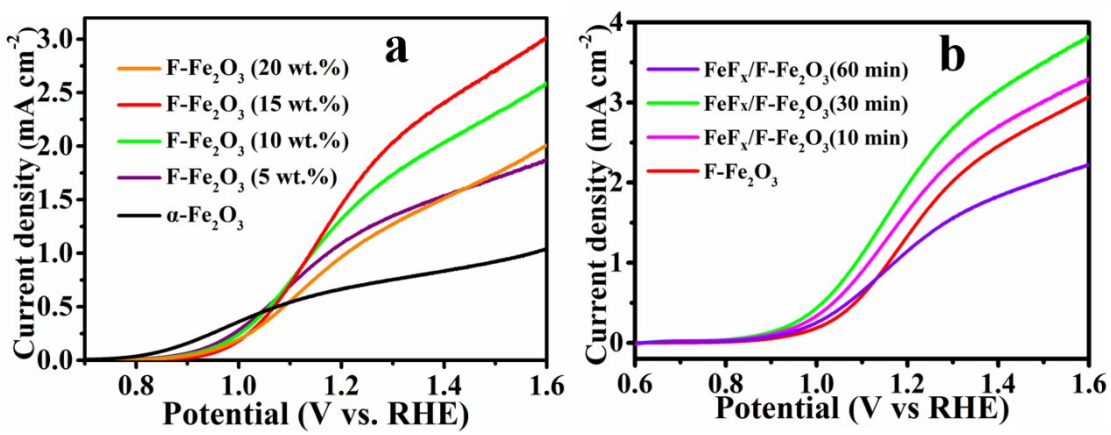


**Fig. S4** LSV plots of F-$Fe_2O_3$ with various F doping amount (a), photocurrent response of $FeF_x$/F-$Fe_2O_3$ with different F-treatment time periods (b).

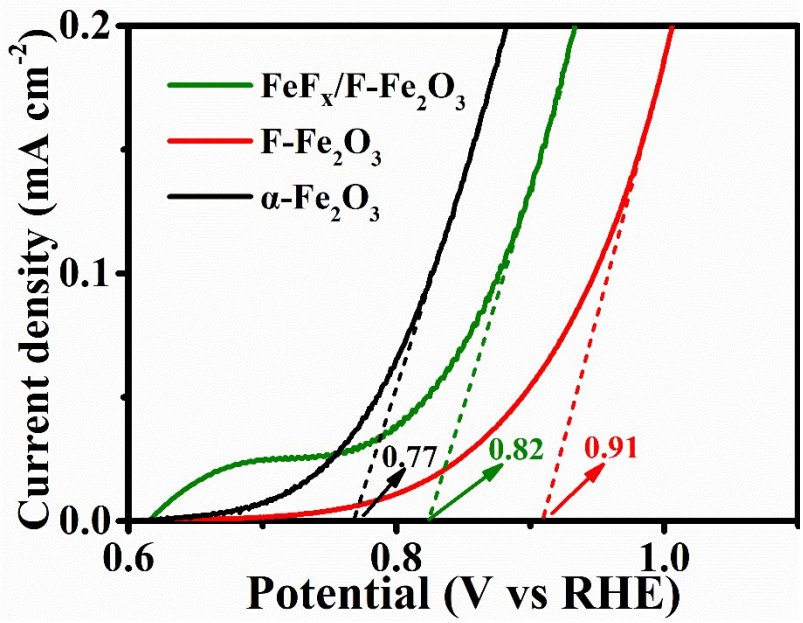


**Fig. S5** Calculated onset potentials of all composite photoanodes.

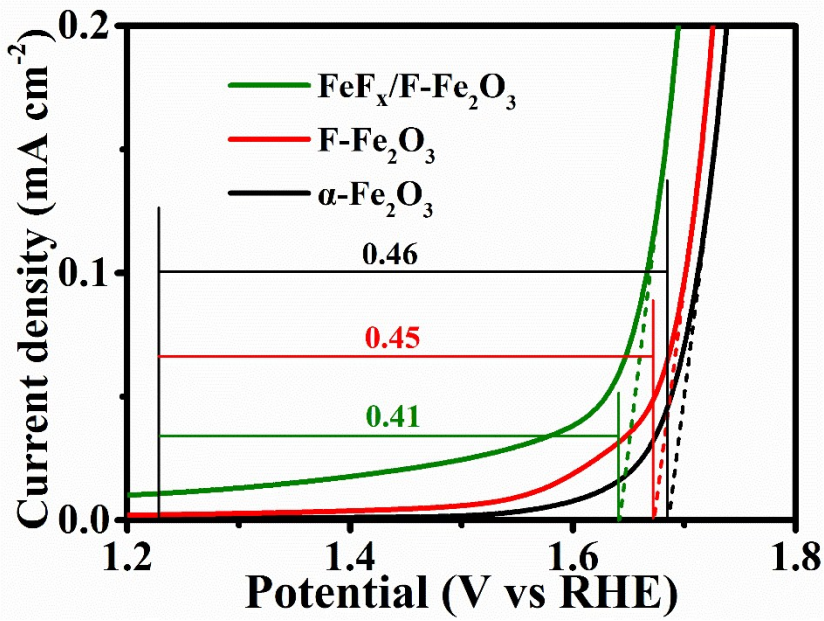


**Fig. S6** Calculated kinetic overpotential of all composite photoanodes.

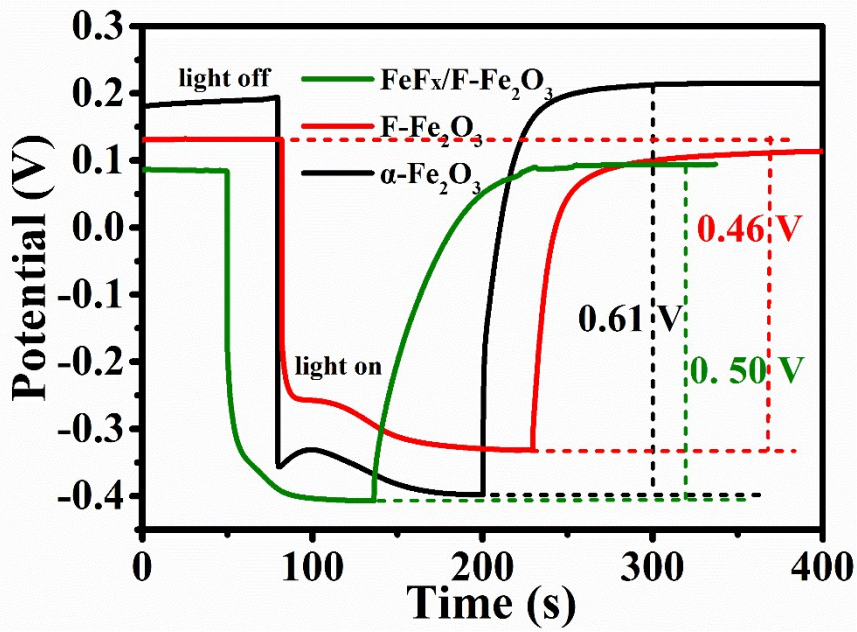


**Fig. S7** Open-circuit potential (OCP) decay curves of each anode and the calculated open-circuit photovoltage ($V_{ph}$) values.

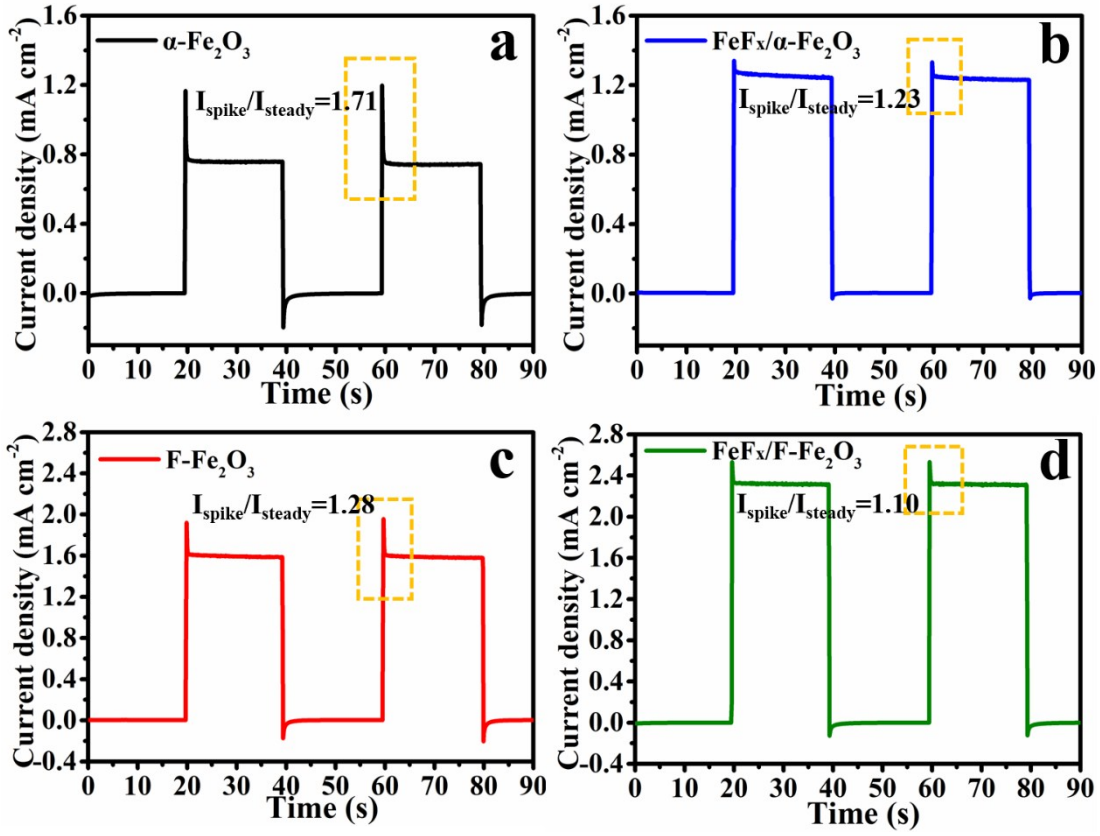


**Fig. S8** The transient photocurrent response of all composite electrodes under chopped illumination at the potential of 1.23 $V_{RHE}$.

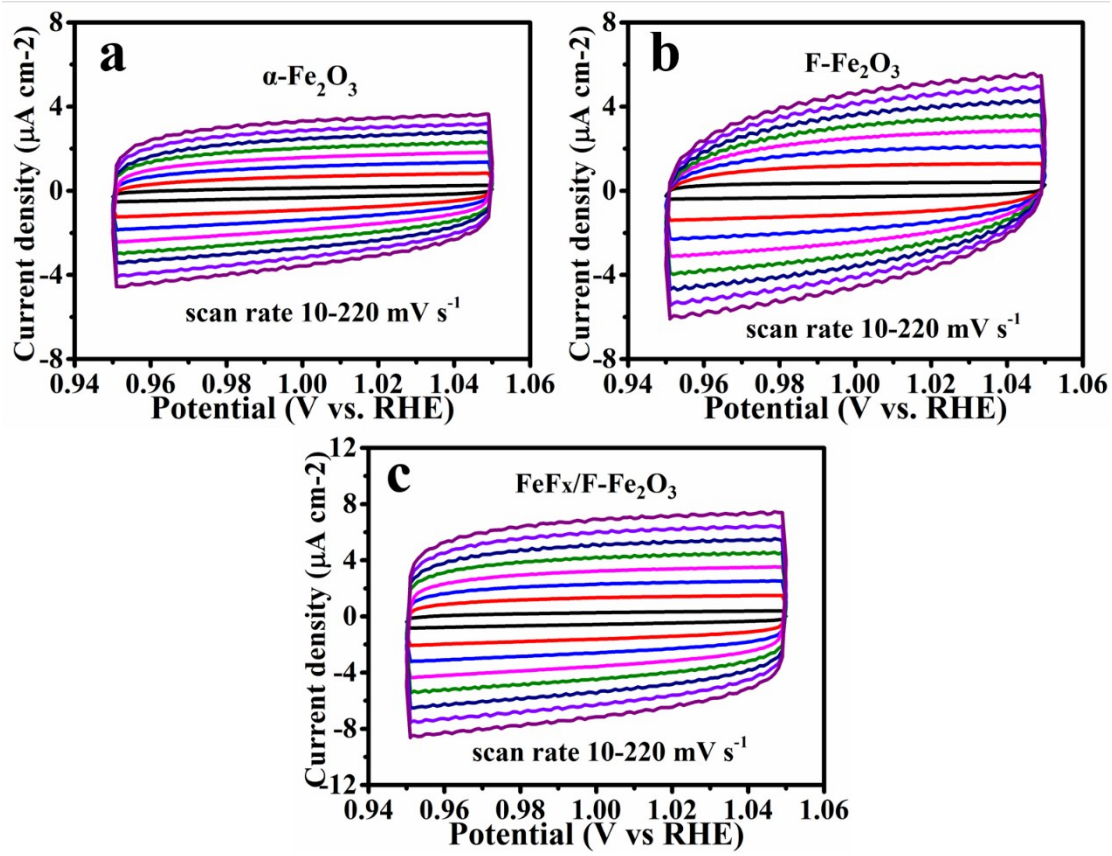


**Fig. S9** Voltammograms of the (A) α-$Fe_2O_3$, (B) F-$Fe_2O_3$, and (C) $FeF_x$/F-$Fe_2O_3$ photoanodes at various scan rates (10-220 mV $s^{-1}$).

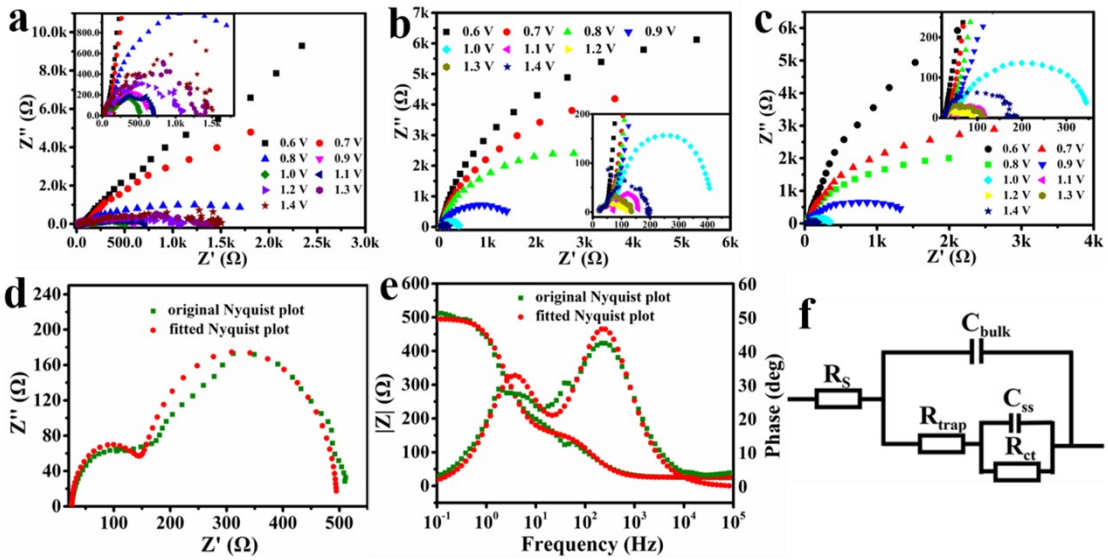


**Fig. S10** The original Nyquist plots of α-$Fe_2O_3$ (a), F-$Fe_2O_3$ (b) and $FeF_x$/F-$Fe_2O_3$ (c) photoanodes obtained at different voltages, the fitted Nyquist plot (d) and bode plot (e) of α-$Fe_2O_3$ at 1.0 V vs. RHE, (f) the equivalent circuit mode used to fit Nyquist plot.

**Table S1. The fitting results.**

| index | symbol | start | end | Error (%) |
|---|---|---|---|---|
| **1** | $R_s$ | 25.71 | 25.71 | 1.452 |
| **2** | $C_{bulk}$ | 1.223E-5 | 1.223E-5 | 2.892 |
| **3** | $R_{trap}$ | 139.1 | 139.2 | 2.567 |
| **4** | $C_{ss}$ | 0.02305 | 0.0002304 | 5.033 |
| **5** | $R_{ct}$ | 330.7 | 330.7 | 2.892 |

Taking the original Nyquist plot of α-$Fe_2O_3$ measured at 1.0 V vs. RHE as an example (Fig. S10d), it consists of two semicircles and exhibits two peaks in the corresponding bode plot. Therefore, an equivalent circuit model consisting of two time constants is employed to fit the original Nyquist plot, which is widely used in the related literatures[6, 7]. In the equivalent circuit mode, $C_{bulk}$ represents the space charge capacitance of the bulk anode, $C_{ss}$ represents the capacitance of surface state, $R_s$ represents the resistance from the electric contact between the electrolyte and electrode, $R_{trap}$ represents the resistance for charge transfer from electrode bulk to surface state, $R_{ct}$ represents the resistance for charge transfer from surface state to electrolyte, respectively[8]. As is shown in Tab. S1, the fitting error is small and within a reasonable range. The two peaks of α-$Fe_2O_3$ in the phase bode plot (Fig. S10e) corresponds to two semicircles in Nyquist plots in Fig. 10d.

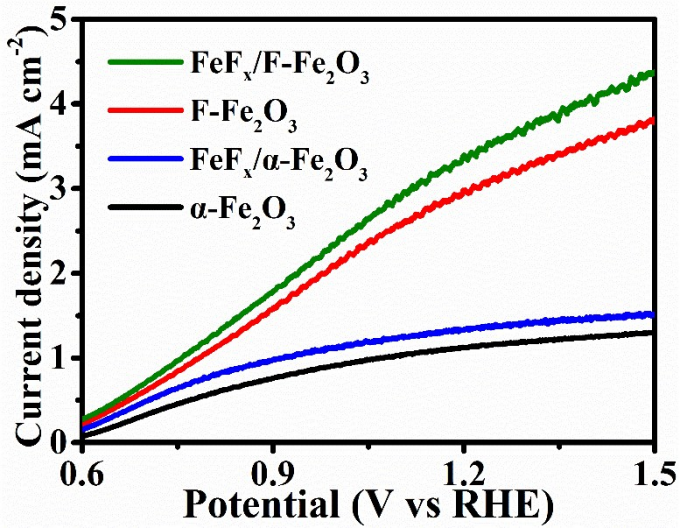


**Fig. S11** LSV plots of each photoanode collected at 5 mV $s^{-1}$ in the solution containing 0.5 M $Na_2SO_3$ and 1 M KOH under one sun illumination (100 mW $cm^{-2}$).

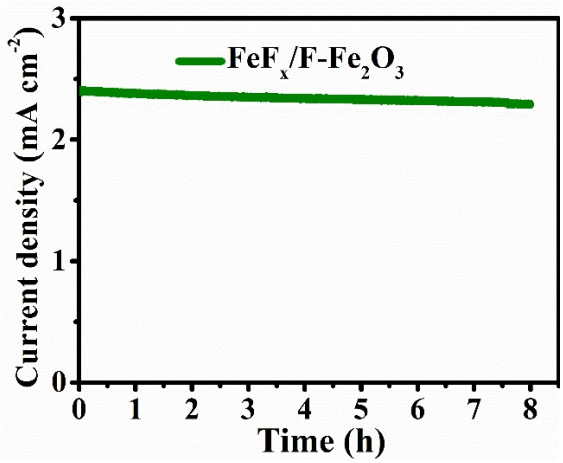


**Fig. S12** Stability measurement curve of the $FeF_x$/F-$Fe_2O_3$ electrode.

**Table. S2** Comparison of our photoanode to other α-$Fe_2O_3$-based photoanode.

| Photoanode | Current density at 1.23 V vs. RHE (mA $cm^{-2}$) | The onset potential (V vs. RHE) | IPCE value | Ref. |
|---|---|---|---|---|
| $FeF_x$/F-$Fe_2O_3$ | 2.41 | 0.82 | 41.5% at 300 nm | This work |
| α-$Fe_2O_3$/Au/$TiO_2$ | 1.05 | 0.86 | 26% at 340 nm | *Applied Catalysis B: Environmental* 260 (2020) 118206 |
| Co-Pi/Ca-$Fe_2O_3$/$Fe_2O_3$/Pt | 2.14 | 0.72 | 53.9% at 390 nm | *ChemSusChem* 2019, 12, 3286 – 3295 |
| Rh-F-$Fe_2TiO_5$/ $Fe_2O_3$ | 2.12 | 0.63 | 37% at 370 nm | *ACS Catal*. 2017, 7, 4062−4069 |
| CoOOH/P:$Fe_2O_3$ | 1.11 | 0.85 | no | *Chemical Engineering Journal* 363 (2019) 23–32 |
| grad P:$Fe_2O_3$/CoPi | 2.0 | 0.8 | 26% at 360 nm | *Chem. Sci*., 2017, 8, 91–100 |
| $FeF_x$–$Fe_2O_3$–Pt | 2.4 | 0.62 | 41% at 350 nm | *J. Mater. Chem. A*, 2018,6, 19342-19346 |
| Mg-$Fe_2O_3$/P-$Fe_2O_3$ | 2.4 | 0.68 | 36% at 300 nm | *J. Mater. Chem. A*, 2018, 6, 13412-13418 |
| Zr-$Fe_2O_3$ NT | 1.50 | 0.89 | 25.7% at 370 nm | *Angew. Chem. Int. Ed.* 2017, 129, 1 – 7 |
| Co-Pi/$Co_3O_4$/Ti:$Fe_2O_3$ | 2.7 | 0.64 | 68% at 400 nm | *Adv. Funct. Mater.* 2019, 29, 1801902 |
| $Fe_2TiO_5$/$Fe_2O_3$/ Pt | 1.0 | 0.97 | 37% at 340 nm | *Adv. Funct. Mater.* 2017, 27, 1703527 |

## Reference


1. L. Gao, F. Li, H. Hu, X. Long, N. Xu, Y. Hu, S. Wei, C. Wang, J. Ma and J. Jin, *ChemSusChem*, 2018, **11**, 2502-2509.
2. F. Li, J. Li, L. Gao, Y. Hu, X. Long, S. Wei, C. Wang, J. Jin and J. Ma, *Journal of Materials Chemistry A*, 2018, **6**, 23478-23485.
3. I. Mora-Seró, F. Fabregat-Santiago, B. Denier, J. Bisquert, R. Tena-Zaera, J. Elias and C. Lévy-Clément, *Applied Physics Letters*, 2006, **89**, 203117.
4. C. Wang, X. Long, S. Wei, T. Wang, F. Li, L. Gao, Y. Hu, S. Li and J. Jin, *ACS Appl Mater Interfaces*, 2019, **11**, 29799-29806.
5. F. Li, J. Li, F. Li, L. Gao, X. Long, Y. Hu, C. Wang, S. Wei, J. Jin and J. Ma, *Journal of Materials Chemistry A*, 2018, **6**, 13412-13418.
6. S.-S. Yi, J.-M. Yan and Q. Jiang, *Journal of Materials Chemistry A*, 2018, **6**, 9839-9845.
7. P. Zhang, T. Wang and J. Gong, *Chem*, 2018, **4**, 223-245.
8. F. Malara, A. Minguzzi, M. Marelli, S. Morandi, R. Psaro, V. Dal Santo and A. Naldoni, *ACS Catalysis*, 2015, **5**, 5292-5300.